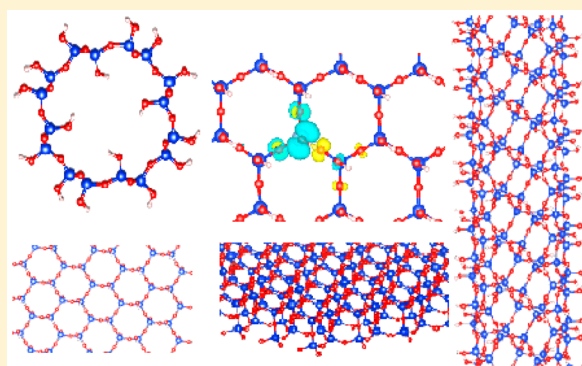# Two-Dimensional Hydrous Silica: Nanosheets and Nanotubes Predicted from First-Principles Simulations

Changming Fang,* Alfons Van Blaaderen, and Marijn A. Van Huis*

Soft Condensed Matter (SCM), Debye Institute for Nanomaterials Science, Utrecht University, Princetonplein 5, 3584 CC Utrecht, The Netherlands

S *Supporting Information*

ABSTRACT: Two-dimensional (2D) hydrous silica sheets (HSSs) and hydrous silica nanotubes (HSNTs) have many unique properties and potential applications. Although preparation of 2D HSSs was patented already about half a century ago, very little is known about their structure and physical properties. Here we predict formations of various kinds of 2D structures. For this purpose, a first-principles study was performed using density-functional theory (DFT) with van der Waals dispersion interaction corrections (optB88-vdW). The uneven hydrous silica sheets and nanotubes have a high stability and are composed of hexagonal rings. The calculations also showed that a bilayer of anhydrous silica sheets is highly stable. Furthermore, the formation of defects which can induce a transition to glassy silica was investigated. The predicted high stability and versatility of these 2D materials offer many opportunities for more extensive developments, including doping with extrinsic elements to functionalize the nanosheets and nanotubes. The present simulation findings pose a challenge to experimentalists for finding useful synthesis routes to access these novel 2D materials.

INTRODUCTION

Two-dimensional (2D) silica structures are highly interesting nanomaterials due to the natural abundance of silica and because of their importance in many fields and in many applications.[1−5] Different techniques have been employed to prepare thinner silica sheets and related nanotubes and nanowires.[1,5−10] Recently Huang and co-workers prepared a thin glassy silica sheet on a graphene substrate. The prepared anhydrous silica sheets have a thickness of a few atoms.[1,6] Björkman and co-workers also reported anhydrous bilayer silica sheets composed of hexagonal rings.[5]

2D silica materials have a long history in the world of colloid science. In the 1960s Wulf invented a method to prepare two-dimensional lepidoid silica sheets with a proposed chemical formula $[(SiO)_6O_3](OH)_6$ or, in a more general form, $[(SiO)_{2n}O_n](OH)_{2n}$.[11] The structural elements within the square brackets form the planar network structure. Each Si has an −(OH) group to satisfy the requirements of tetragonal coordination and charge balance. That indicates that the structure of the hydrous silica sheets has to fit the Zachariasen's network model (with Si sp^3 bonding).[12] Though both having hexagonal rings, the SiO$_4$ sp^3 in the rings in the uneven sheets is different from the C−C (sp^2 bonding) in the well-known graphene flat plane.[13] The sizes of the two-dimensional silica sheets prepared in this way range from nanometers to 100 μm depending on the control over preparation conditions (pH value, temperature, solutions, etc.).

It is expected that this type of hydrous silica sheet has unique properties and potential applications. First, the −(OH) groups are chemically very active and may react with different clusters or ions to form desired functional materials. Second, the large surface to volume ratio together with the attachments of metal ions implies opportunities for the two-dimensional silica sheets to be employed as hosts or supports for highly efficient nanocatalysts or two-dimensional luminescent materials. Third, the porous nature of the silica sheets with different sizes of holes adjusted by different ions also implies possible usage as membranes to separate different ions or gas molecules. Furthermore, the 2D structure of the hydrous silica provides opportunities for building various shapes of nanosized to microsized materials, such as tubes, spheres, cubes, mesoporous silica, etc.[14−18] These building blocks are of scientific interest to understand the nature of silica colloids[17−19] and the formation of biomaterials.[2−4] Finally, the insulating nature of the 2D silica sheets/tubes may well be of interest for potential application as atomically thin electrical barriers in nanoelectronic systems. For further development, detailed knowledge of the structure, stability, and properties of the hydrous sheets is required. However, at present there is hardly any clear information about the geometry, chemical bonding, stability, and properties of 2D
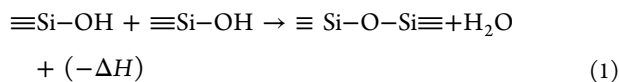
hydrous silica sheets (HSSs) and hydrous silica nanotubes (HSNTs).

Theoretical efforts have been performed but were limited mainly to anhydrous two-dimensional silica sheets and related tubes and nanowires.[5,8,2−23] Through a combination of first-principles and classic force field calculations, Björkman and co-workers investigated anhydrous hexagonal silica bilayer sheets,[5] and Weissenrieder and co-workers simulated the geometry of hexagonal silica sheets on metal surfaces.[8] Zhao and co-workers studied anhydrous silica sheets and related tubes using first-principles calculations,[21] whereas De Leeuw and co-workers investigated hydration effects on anhydrous silica tubes.[23] *Ab initio* and first-principles studies have also been applied for silicic acid molecules and clusters.[24−27] To the best of our knowledge, to date theoretical studies on 2D hydrous silica sheets have not yet been reported.
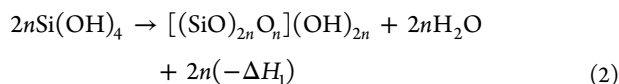
In the present manuscript, we show the results of a first-principles study of 2D hydrous silica sheets starting from the work of Wulf,[11] using density functional theory (DFT) within the van der Waals density functional approximation. HSNTs are designed with a diameter of about 1.2 nm based on the hydrous silica sheets. For the sake of comparison, 2D anhydrous silica sheets and nanotubes with hexagonal rings or squares were also simulated. Electronic properties were studied at the level of density functional theory. Defects, Si−O−Si bond breaking, and dilute Al doping were considered to address the noncrystalline nature of colloid materials at elevated temperature and the relevance to the important class of zeolite materials. Geometry, important interatomic distances, chemical bonding, net charges, and charge transfer in these systems are addressed. The obtained knowledge here is useful not only to understand the structural properties and chemical bonding of the silica sheets but also more generally to get insight for silica sol gels and related materials, such as zeolite,[28] and to develop novel materials of interest to catalysis, bioscience, and materials science.[2−4,29,30]
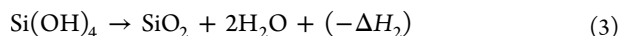
■ COMPUTATIONAL METHODS

Formation Energy of Silica. The reactions of formation of silica from silicic acid occur during water condensation processes with the general formula[19,26−31]

$$\equiv Si-OH + \equiv Si-OH \rightarrow \equiv Si-O-Si\equiv + H_2O$$
$$+ (-\Delta H) \tag{1}$$

For the formation of hydrous silica sheets the reaction is

$$2n Si(OH)_4 \rightarrow [(SiO)_{2n}O_n](OH)_{2n} + 2n H_2O$$
$$+ 2n(-\Delta H_1) \tag{2}$$

For the formation of anhydrous silica from silicic acid, the water condensation reaction is

$$Si(OH)_4 \rightarrow SiO_2 + 2H_2O + (-\Delta H_2) \tag{3}$$

In this way the formation enthalpies (ΔH_1 and ΔH_2) are expressed per Si in the reactions 2 and 3. This can be used to determine the relative formation enthalpy of different reactions and can be used as a measure of stability. Negative values of (ΔH_1 and ΔH_2) represent favorable reactions, while positive values mean that the reactants are favored. In our calculations we evaluate total valence electron energies for the silicic acid and water molecules and the condensed products at the ground states. The formation energies of the reactions can be obtained

from these equations. At a temperature of 0 K and a pressure of 0 Pa, the formation entropy (ΔH) is equal to the formation energy (ΔE) when zero vibrational energy contributions are not taken into account.

Simulation Cells. In the plane-wave DFT approach (details will follow in the next subsection), periodic boundary conditions apply, and appropriate supercells need to be constructed. Cubic supercells with axis lengths of 20.0 and 16.5 Å were used for a silicic acid molecule and a water molecule, respectively. In this way the distances between molecules in neighboring supercells are longer than 14 Å, large enough to avoid intermolecular interactions. Results are listed in Table S1 in the Supporting Information (SI).

The inputs of structures of both anhydrous and hydrous silica sheets were built within different unit cells with two-dimensional periodicity. The starting primitive cell is hexagonal with lattice parameter $a_0 \sim 5.1$ Å and contains two Si atoms with chemical composition $[(SiO)_2O](OH)_2$ for hydrous silica sheets, whereas for anhydrous sheets the primitive cell is cubic, starting with $a_0 \sim 3.0$ Å which contains one SiO_2 unit. Considering the flexibility of silica, we also tested $2a_0 \times 2a_0$ and $3a_0 \times 3a_0$ supercells. The results showed that the $2a_0 \times 2a_0$ supercells are large enough for the anhydrous silica sheets; meanwhile, for the hydrous silica sheets the total energy of the primitive cell is close to those of larger supercells, probably due to compensation of the $-(OH)$ clusters. The $3a_0 \times 3a_0$ supercell was also employed for defect calculations. The lengths of the c-axis perpendicular to the sheets are larger than 24 Å, which is sufficient to avoid intersheet interactions.

van der Waals Functional and Computational Settings. The standard first-principles density functionals, such as local density approximation (LDA) and generalized gradient approximations (GGA), do not take into account van der Waals interactions,[32,33] which results in lower accuracy results for sparse systems such as the silica sheets. Therefore, we have employed the van der Waals density functional formulated by Dion and co-workers[33,34] for the silica systems. The van der Waals functional was implemented in many first-principles codes[34−37] including the VASP code (Vienna ab initio simulations package),[38−40] which has been employed for all the calculations in the present work. This approach is based on the optimized PBE approximation with the London dispersion interaction for the nonlocal electron correlation effects (optB88-vdW) which has been successfully applied for various systems.[34−39] Both spherical and nonspherical contributions from the gradient corrections inside the atomic spheres are included.[40] The electronic wave functions were sampled on dense grids for calculation of the total energy and the electronic structure. A $12 \times 12 \times 2$ grid with 148 irreducible k-points in the Brillouin zone (BZ) was used for the 2D graphite-type hydrous silica sheet and the anhydrous bilayer silica sheet, and the $10 \times 1 \times 1$ grid with 5 irreducible k-points in the BZ was used for the 1D hydrous silica tubes and for the 1D anhydrous silica tubes, employing the Monkhorst and Pack method.[41] An "only Γ-point" setting was employed for the isolated molecules. Structural optimizations were performed for the 2D sheets with fixed lattice parameters to find the *a*- and *b*-axis at the systems' energy minima, while only the atomic coordinates in a fixed cube were relaxed for the single-molecule calculations. We also used the fixed volume approach to determine the lattice parameters of the two periodic dimensions from the minimized total energies. The optimizations showed that the two approaches produced the same results within the accuracy of

our calculations. Note that, in principle, all valence electrons belong to the whole crystal. However, we can decompose the plane waves in the spheres and obtain their corresponding components in the spheres. In this way the partial density of states at an atom is obtained.

The molecules and silica sheets in the present study contain strong local bonds, such as 2p−3p (e.g., Si−O) or 2p−1s (e.g., O−H) bonds, and therefore, the calculated valence electron total energy is expected to depend on the cutoff energies. This indicates that high cutoff energies for the electron wave functions are required. In the present work the cutoff energy of the wave functions was set at 750 eV, and the cutoff energy of the augmentation wave functions was at 1000 eV. Tests of k-mesh and cutoff energies showed a good energy convergence (<1 meV/atom).

■ RESULTS AND DISCUSSION

A. 2D Silica Sheets. Structural optimizations were performed for various configurations of hydrous silica sheets. The calculations showed that for the primitive cell the one with −(OH) clusters on only one side of the sheet is favored (Figure 1(f,g)). To have a better understanding about the effects of
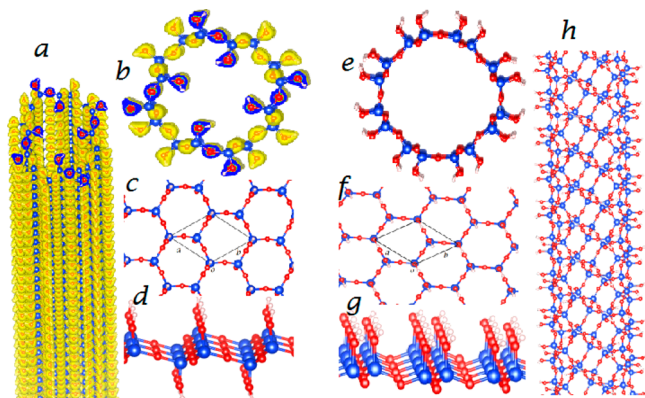

Figure 1. Schematic structures of hydrous silica sheets (HSSs): (c,d) are for one HSS with −(OH) groups on two sides and (f,g) for an HSS with −(OH) clusters on one side. Hydrous silica nanotubes (HSNTs): (a) and (b) show the electron density isosurfaces for a HSNT with 1/3 of the −(OH) clusters pointing inward, while (e) and (h) show an HSNT with all −(OH) clusters pointing outward. The blue spheres represent Si atoms, the red spheres O atoms, and the small white spheres H atoms.

−(OH) cluster distributions, we also performed calculations for the geometry and energetics of −(OH) cluster distributions in a $2a_0 \times 2a_0$ supercell for the hydrous silica sheets. The results from the supercell confirmed the conclusion that the configuration with −(OH) clusters on one side is preferred. These results indicate that at a larger scale −(OH) clusters will form domains at both sides of the sheet. Figure 1(c,d) also shows hydrous silica sheets with an even −(OH) distribution.

Structural analysis showed that all the O atoms/ions in the hydrous silica structures play a role of bridging H and Si atoms or bridging Si atoms. A typical case is shown in Figure S1 of the Supporting Information (SI) where Si atoms are in distorted tetragons with the O−Si−O angles deviating within 3° from the 109.5°, the bond angle in a regular tetragon. The angle Si−O−H is calculated to 118.2°, being close to that in a silicic acid molecule, 118.5° (Figure S1, SI).

The silica sheets can also be formed into nanotubes, for which many possibilities exist. Here we designed a nanotube with a diameter of about 1.2 nm. Different distributions of −(OH) clusters were considered (Table 1). The calculations showed that the most stable configuration (Tube 3) has one-quarter (4/16) of the (OH) clusters pointing inward as shown in Figure 1(a,b). Its formation energy is indicated with the lowest violet sphere in Figure 2. The tube configuration which follows in stability is the configuration with all −(OH) clusters pointing outward (Tube 1 in Table 2, Figure 1(e,h)).

The total energy calculations showed that the formation energies of the HSSs and HSNTs are favored over the silicic acid molecules (Table 1 and Figure 2). The HSS with −(OH) clusters on one side is the most stable configuration, whereas the HSNT with one-quarter of the −(OH) clusters pointing inward is also highly stable (Table 1 and Figure 1(a,b)). Overall, the obtained formation energies as defined in eq 2 are in the range between −0.23 eV and −0.34 eV/Si for the HSNT and HSS from the calculated total energies in Table 1. The calculations also showed that when more −(OH) clusters (e.g., half of them) are pointing inward the tubes become structurally unstable.

B. Anhydrous Silica Sheets and Tubes. To have a better understanding of hydrous silica sheets and tubes, we also investigated two-dimensional *anhydrous* silica sheets not having any hydrogen atoms. The results are listed in Table 2. From the previous section, it became clear that the hydrous silica sheet with −(OH) clusters distributed on one side has a high stability. This provides an opportunity to create a bilayer anhydrous silica sheet with hexagonal rings, as proposed by Björkman and co-workers.[5] The schematic structure is shown in Figure 3(a,b).
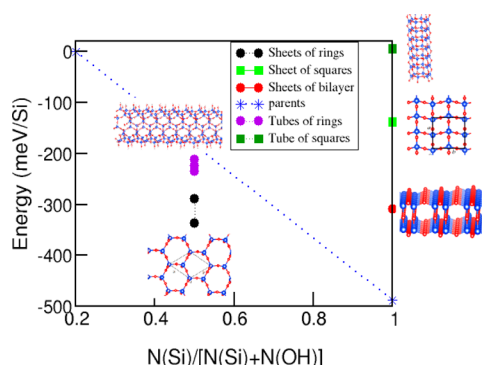
First a simple square unit cell with the lattice parameter a_0 is built. This cell contains one SiO_2 molecule with one Si atom at the center (0.5, 0.5, 0) and two O atoms at the line centers (0.5, 0, $z1$) and (0.0, 0.5, $z2$), with both $z1$ and $z2$ slightly deviating from 0 to link two Si atoms. In this way each Si atom is connected to four O atoms. The z-coordinates are used because of the preferred tetragonal coordination of Si (sp^3 hybridization). Structural optimizations and total energy calculations were performed, and it follows according to eq 3 that this structure is unstable relative to isolated silicic acid and water molecules (Table 2).

We also employed a supercell approach and relaxed both atomic coordinates and lattice parameters at a fixed volume. The optimization resulted in different lengths of a- and b-axes (Table 2). The formation energy found from the calculations is about −0.138 eV/SiO_2 relative to silicic acid and water as defined in eq 3. This indicates that this anhydrous silica sheet is favored over the silicic acid molecules. However, this formation energy is smaller than that of the 2D HSSs (Table 1) and significantly smaller than that of quartz (Table 2). The optimized structure is shown in Figure 3(c,d). It is clear that the anhydrous silica sheet is strongly buckled and can be characterized by two Si chains with O atoms. All O atoms are bridging the Si atoms. The Si atom is in a distorted tetragonal coordination by O atoms as shown in Figure S1 (SI). Most of them have O−Si−O angles of around 108°, which is smaller than 109.5° (the angle in a regular tetragon), while the O−Si−O angles for the outer O atoms via the Si are notably larger (about 115°).

From Table 2 it becomes also clear that the calculations show a high stability of bilayer anhydrous silica sheets (Figure 3a,b)

Table 1. Optimized Results (Lattice Parameters, Chemical Bonding, Net Charges and Total Valence Electron Energies, As Well As Calculated Formation Energies According to Equations 2 and 3) for the Most Stable HSSs and HSNTs[a]

	lattice pars. (Å)	$d(Si-O)$ (Å), $d(O-H)$ (Å)	charge	ΔE (eV/Si)
hydrous silica sheet $(Si_2O_3(OH)_2)$, hexagonal lattice				
−OH clusters at two sides	$a = 5.184$	Si−O(1): 1.62(×3)	Si: 3.20	−0.289
	$Z = 1$	−O(H): 1.64	O(Si): −1.60	
		H−O(H): 0.97	O(H): −1.40	
			H: 0.61	
−OH clusters at one side	$a = 5.292$	Si−O(1): 1.62(×3)	Si: 3.19	−0.336
	$Z = 1$	−O(H): 1.65	O(Si): −1.61	
		H−O(H): 0.97	O(H): −1.39	
			H: 0.61	
hydrous silica tubes based on hydrous silica sheet $(Si_2O_3(OH)_2)$				
Tube 1: all −OH clusters pointing outward	$a = 5.262$	Si−O(1): 1.62(×3)	Si: 3.18	−0.223
	$z = 8$	−O(H): 1.64	O(Si): −1.59	
		H−O(H): 0.97	O(H): −1.40	
			H: 0.60	
Tube 2: 1/16 of −OH clusters pointing inward	$a = 5.262$	Si−O(1): 1.63(×3)	Si: 3.17	−0.211
	$z = 8$	−O(H): 1.65	O(Si): −1.59	
		H−O(H): 0.97	O(H): −1.40	
			H: 0.59	
Tube 3: 1/4 of −OH clusters pointing inward	$a = 5.262$	Si−O(1): 1.63(×3)	Si: 3.17	−0.235
	$z = 8$	−O(H): 1.65	O(Si): −1.59	
		H−O(H): 0.97	O(H): −1.40	
			H: 0.59	

[a]The hydrous silica sheet $(Si_2O_3(OH)_2)$ has a hexagonal lattice.

Figure 2. Calculated formation energies as defined by eq 2 for hydrated silica nanosheets and nanotubes (HSSs and HSTs) and by eq 3 for anhydrous silica sheets and tubes. If multiple symbols of the sample color (detailed in the legend) are plotted, they represent configurational variations of a particular structure, such as the variation in the number of inward/outward pointing (OH) groups in the hydrous silica nanotubes, as listed in Table 1 and described in the text. The "parents" represent a silicic molecule and quartz.

when compared to the other formation energies listed in Tables 1 and 2. This indicates that for silica sheets the bilayer sheet is the most likely to be formed by physical approaches, such as plasma evaporation.[1,5,6] However, the growth of the two-dimensional hydrous silica sheets typically takes place in solution,[11] and under such conditions one expects that the formation of the hydrous sheets is more likely than the formation of anhydrous sheets. The small formation energy for the anhydrous silica tube (Table 2, configuration shown in Figure 3e) also indicates that this phase may be difficult to synthesize when compared to the hydrous silica nanotubes. This is also clear from Figure 2, which includes the formation energies of both hydrous and anhydrous nanotubes.

C. Electronic Properties of Hydrous Silica Sheets. We performed electronic structure calculations for the hydrous silica sheets and tubes. The calculations showed strong similarity for the various sheets and nanotubes. The dispersion curves of the most stable anhydrous silica bilayer and the hydrous silica tube with a quarter of the −(OH) groups pointing inward are shown in Figure S3 of the Supporting Information. Here we present the results for the more stable one with −(OH) clusters on one side. The partial and total density of states (DOS) and dispersion curves are shown Figure 4.

The electronic structure of hydrous silica consists of four separated bands (as shown in Figure 4). All valence bands are dominated by O 2s (from −19.5 to −16.9 eV) and 2p states (from −9.5 to 0 eV, the Fermi level). The O1 2s states are dominating the bottom and the top parts of the O 2s states with the O(−H) 2s states also contributing, with a peak at about −18.0 eV. The dispersion of these bands is 0.5−1.0 eV. Such dispersions are quite large considering the semicore nature of the O 2s states. The second lowest band is composed of O 2p states mixed with Si 3s, 3p, and H 1s characters. This is the bonding band. The third band, the valence band ranging from −3.7 to 0.0 eV (the Fermi level), consists of mainly the O 2p states (nonbonding orbitals). It is noted that the top of the valence band is dominated by the nonbonding 2p states of the O ions bridging two Si ions. There is an energy gap of about 5.5 eV between the valence band and the conduction band. The calculations also showed that for the conduction band the densities of the partial s and p states of Si, O, and H are notably smaller than that of the total DOS (Figure 5). This is due to the fact that we have to employ small spheres for O (0.82 Å) due to the short O−H bond length. Therefore, the decomposition of the orbitals produced too low densities for O 2p orbitals. However, this artifact has no impact on our understanding of the nature of the conduction band. There is a direct band gap at

Table 2. Calculated Anhydrous Silica Single-Layer Sheets, A Single-Wall Square Nanotube, and a Bilayer Silica Sheet with Hexagonal Rings[a]

unit cells	lattice	d(Si–O) (Å)	charge (e)	ΔE (eV/SiO$_2$)
	anhydrous silica sheets and a nanotube (single-layer)			
primitive cell	square			+0.361
	$a_0 = 2.846$	1.66(×4)	Si$^{+3.10}$(O$^{-1.55}$)$_2$	
	$Z = 1$			
supercell $2a0 \times 2b0$	orthorhombic			−0.138
	$a = 5.022$	1.63(×2)	Si$^{+3.19}$(O$^{-1.59}$)$_2$	
	$b = 5.545$	1.65(×2)		
	$Z = 4$			
nanotube with squares	$a = 5.6452$	1.63(×2)	Si$^{+3.20}$(O$^{-1.59}$O$^{-1.61}$)	−0.019
	$Z = 8$	1.65(×2)		
	anhydrous bilayer silica sheet with hexagonal rings			
supercell	hexagonal			
	$a = 5.292$	1.63(×4)	Si$^{+3.20}$(O$^{-1.60}$)$_2$	−0.332
	$Z = 4$			
crystalline silica (α-SiO$_2$ quartz)	hexagonal			
	$a = 4.982$	1.627(×4)	Si$^{+3.21}$(O$^{-1.61}$)$_2$	−0.549
	$c = 5.485$			
	$Z = 3$			

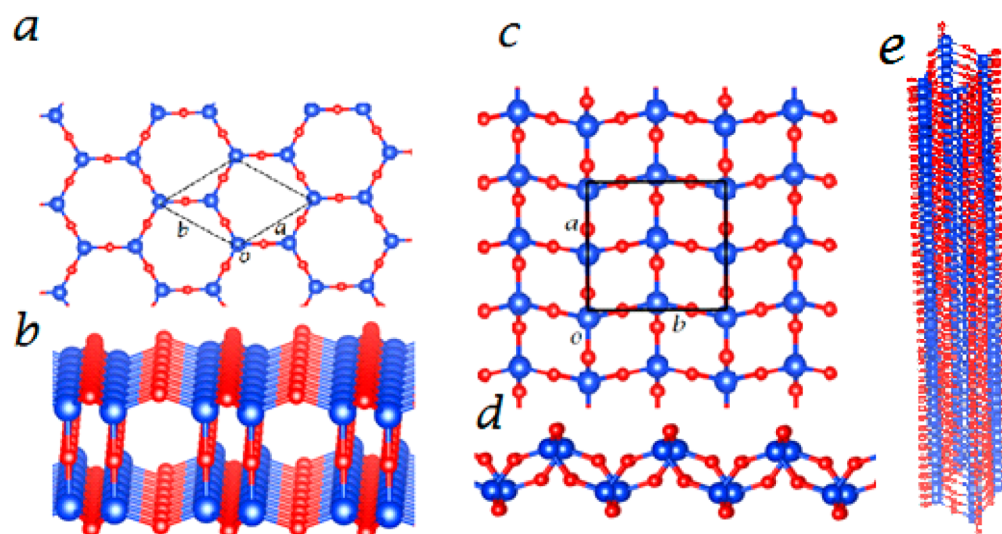[a]The formation energies are defined relative to silicic acid and water as formulated in eq 3.

Figure 3. Relaxed structures for (a,b) an anhydrous silica bilayer sheet with hexagonal rings; (c,d) single-layer sheet with squared network; and (e) a single atomic layer silica tube with square cross-section (also see Figure S2, SI). The blue spheres represent Si atoms and the red spheres O atoms. The color coding is the same as in Figure 1.

the center of the Brillouin zone (Γ point, Figure 4b). It is expected that this band gap will be smaller than experimental value, considering the fact that density-functional theory underestimates the band gaps of insulators.[33,42−44]

As shown in Figure 4 the densities of Si 3s 3p states are much smaller than those of the corresponding O 2s 2p states. This can also be observed in the electron density distributions in Figure 4c. This is due to the ionic nature of the compounds. The Si ions are close to purely ionic with a charge of about 3.2 e (Tables 1 and 2). The densities of both Si 3s and 3p are mainly in the second band (the bonding band). The hybridization of both Si 3s and Si 3p states with oxygen corresponds to the sp^3 bonding nature of silica. Figure 4 also shows that the H and nearby O are strongly bonded (Figure 4c). It is difficult to clearly separate the two ions/atoms, which is the reason that an −(OH) cluster behaves as an ion.

D. Defects and Noncrystalline forms of the 2D HSSs.

As shown in Table 2, the most stable form of silica at ambient conditions is quartz. However, it is well-known that quartz cannot be formed with conventional preparation techniques. Most chemical and physical preparations result in noncrystalline or glassy structures of silica. 2D configurations of glassy bilayer silica sheets with hexagonal rings were previously obtained experimentally.[1,5,6] Therefore, we should also consider the noncrystalline nature of 2D HSSs.

Most silica sol−gel structures are formed in solutions at elevated temperature. That indicates that under these preparation conditions a balance of reactions is reached at equilibrium. Therefore, it is of chemical interest to consider the reverse reaction of water condensation, that is, water hydrolysis, through which a 2D silica sheet is formed as follows
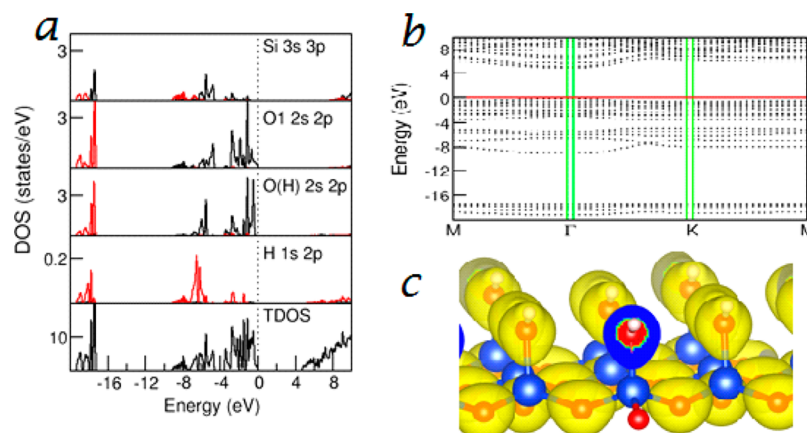
Figure 4. Partial and total density of states (a), dispersion curves of the band structure (b), and the electronic-density iso-surfaces of the hydrous silica sheet (c). The curve at the bottom in (a) shows the total density of states (TDOS); the curves above the TDOS show the partial density of states (pDOS); whereby the red lines represent the s characters of Si or O and the black lines the p characters. The strong O−H covalent bonding and the ionic nature of Si can be easily recognized. In panel (c), the blue spheres represent Si atoms, the red spheres O atoms, and the small white spheres H atoms.
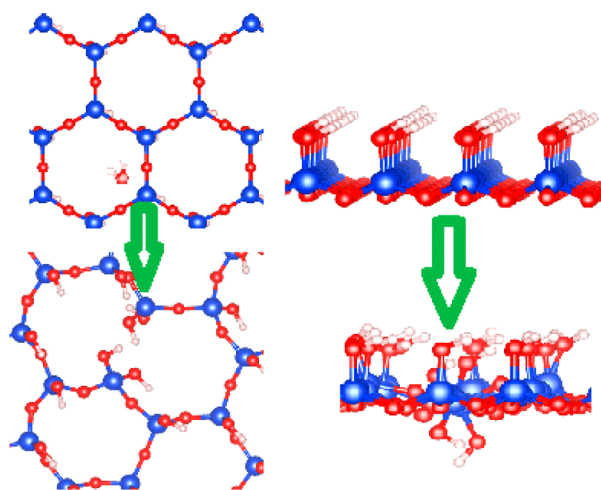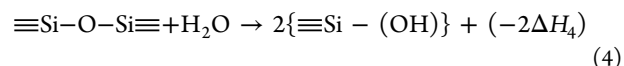

Figure 5. Optimized local structure of 2D-HSS with one Si−O−Si bond reacting with a water molecule (water hydration, eq 1), which produces a locally distorted structure. The local disorder may lead to the formation of glassy 2D HSSs.

$$\equiv\!Si-O-Si\!\equiv\; + H_2O \rightarrow 2\{\equiv\!Si-(OH)\} + (-2\Delta H_4)$$

(4)

where $-2\Delta H_4$ is the reaction enthalpy to break a $\equiv\!Si-O-Si\!\equiv$ bond and to form two $-(OH)$ clusters using one water molecule. To perform point defect calculations for a broken Si−O−Si bond, a $3a_0 \times 3a_0$ supercell (here a_0 is the lattice parameter of a primitive cell) was employed. The optimized structure of the 2D HSS with one broken Si−O−Si bond is shown in Figure 5. One broken Si−O−Si bond in the hydrolysis reaction produces two $\equiv\!Si-(OH)$ with the $-(OH)$ clusters pointing toward the opposite side of the original $-(OH)$ clusters. Figure 5 also clearly shows that the water hydrolysis reaction results in strong local relaxations. Compared to the well-ordered 2D HSS, the Si atoms/ions with two $-(OH)$ clusters are out of the Si atomic plane. The nearby O and $-(OH)$ clusters also show notable distortion. This suggests that a large concentration of such defects will lead to amorphization.

Electronic total energy calculations also provide the total valence electron energies for each of the related systems. The calculations showed that in the hydrolysis reaction it takes an enthalpy $(-2\Delta H_4)$ of about 0.368 eV to break one Si−O−Si
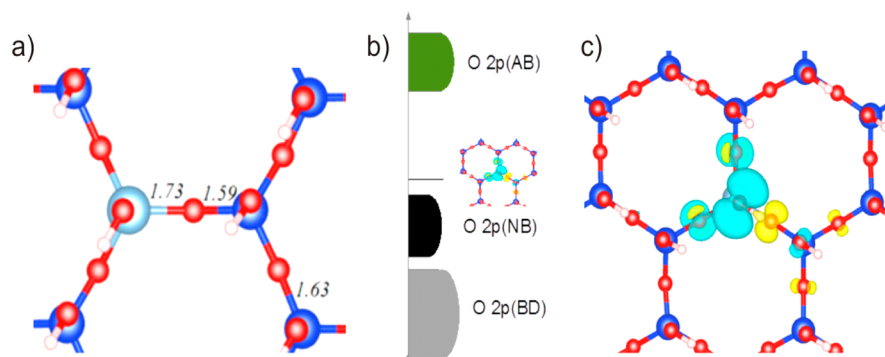

Figure 6. (a) Schematic local structure with M−O bond lengths (Å) indicated. (b) Schematic electronic structure of a HSS with Al doping. The type of bonding is indicated next to the bands. BD: bonding; NB: nonbonding; AB: antibonding. The valence bands are composed of the bonding O 2p states (gray) and the nonbonding O 2p states (black). The conduction band is dominated by antibonding O2 2p states (green). The Al doping produces a narrow band (acceptor) of impurity states (the black line). (c) Isosurfaces show the spin polarization of the O 2p ions near Al (see text for details).

bond and to react with one water molecule to form two $-Si-$ (OH) groups or 0.184 eV to produce one Si(OH) termination, as given in eq 4. However, under hydrolysis conditions and at elevated temperature, this reaction may well require much less energy.

In the field of catalysis, zeolites which contain metallic ions, such as Ca, Mg, and Al, are widely used. Here we consider only a simple case and replace one Si by Al in a $3a_0 \times 3a_0$ supercell (here a_0 is the lattice parameter of a primitive cell). The geometry optimizations produced the following local chemical bonds for the tetragonally coordinated Al (Figure 6a); for the in-plane Al—O: 1.73 Å (×3) and 1.78 Å for the Al—O bond to the (OH) cluster. The related Si—O bonds have notably shorter lengths (1.59–1.60 Å) in comparison to the other Si—O bonds (about 1.63 Å, Tables 1 and 2). Bader charge analysis showed that the Al atom, which has three valence electrons, is charged by +2.46 electrons, in agreement with the ionic nature of alumina, whereas the neighboring O atoms/ions are charged with -1.48 e for the in-plane O and -1.16 e for the O in the (OH) cluster, respectively. These values are notably smaller than those nearby Si atoms. This is understandable since the Al atom has one electron less than Si.

Electronic structure calculations showed that the Al defect exhibits spin-polarization, which is situated at the O atoms that are nearest neighbors to the Al atom in the doped HSS. The three in-plane O atoms in plane are slightly spin-polarized with a local moment value of about 0.04 μ_B, while the O in the (OH) cluster has a significant local moment of about 0.24 μ_B, which is clearly shown in Figure 6c. It is also notable that the magnetic moment (in yellow) of one of the in-plane O atoms is antiparallel to the rest. The calculations also showed that the acceptor state is about 0.2 eV above the top of the valence band.

Further Discussion and Outlook. The challenge that lies ahead is to realize experimentally the predicted 2D HSSs, HSNTs, as well as the bilayer silica sheets of high stability. Recent reports of experimentally prepared bilayer silica sheets showed that the structures have a significantly amorphous nature.[1,5,6] A similar noncrystalline nature may exist for the HSSs and HSNTs.

The predicted 2D silica sheets of high stability showed a clear atomic ordering, but the calculations also showed that defects, in particular Si—O—Si bond breaking by water condensation and Al doping, can cause significant local relaxations and symmetry breaking. As pointed out by many, the formed silica materials are strongly dependent on the preparation conditions. For example, one expects that in acidic solutions an Al atoms/ion doped in a HSS/HSNT is likely to lose its (OH) cluster and become three-coordinated to reach charge balance. Meanwhile in a base solution, the Al ion/atom is likely to attract one —(OH) cluster in solution and is 4-coordinated with an unoccupied hole in its local electronic structure. The control over sizes and shapes of the hydrous silica sheets by adjusting preparation conditions such as temperature, pH-value, solution parameters, etc., as pointed out by Wulf[11] provides a valuable opportunity to synthesize the structures predicted in the current work. Also, synthesis of silica on top of a suitable atomic template, as is currently done to synthesize graphene nanoribbons,[47] could provide a successful synthesis route.

The current findings open a wide window of opportunities for further development with a broad range of possible applications. For example, one may deposit the hydrous silica sheets onto nanocrystals (NCs) to reach the ultimate goal of atomic coating by means of suitable sol—gel approaches. The charge and spin-polarization of Al doped 2D silica sheets/tubes may play an role in the catalysis processes containing magnetism, e.g. for chemical reactions involving magnetic O_2 molecules, considering that reaction barriers will be substantially lowered due to angular momentum conservation.[45,46] Therefore, this type of hydrous silica sheets deserves further experimental and theoretical investigations. Also the dynamical stability of these structures may be investigated by phonon dispersion calculations and molecular dynamics simulations in future studies.

CONCLUSIONS

Structure, stability, and electronic properties of two-dimensional hydrous silica sheets and nanotubes were simulated using the first-principles DFT approach. In the hydrous silica sheets and nanotubes, each Si is in a distorted tetragonal coordination and has three Si—O bonds in the sheet and one OH cluster pointing outward. Total energy calculations showed a high stability of the 2D hydrous silica sheets and nanotubes, as well as 2D anhydrous bilayer silica sheets of hexagonal rings. A relatively low energy is required to break a Si—O—Si bond, which is indicative of how easily the structures can be amorphized. Electronic band structure calculations showed that hydrous silica sheets are wide-gap insulators with band gaps over 5.5 eV. Interestingly, the doping of Al causes spin-polarizations of the neighboring O atoms. However, the knowledge about the 2D silica sheets and nanotubes is still far from complete, and much more extensive experimental and theoretical studies should be performed. The versatility of these 2D materials offers many opportunities for developing applications in various fields such as nanoelectronics, catalysis, and biomaterials science. The present simulation findings pose a challenge to experimentalists for finding useful synthesis routes to access these novel 2D materials.

ASSOCIATED CONTENT

Ⓢ Supporting Information
Table S1 and Figures S1–S3. The Supporting Information is available free of charge on the ACS Publications website at DOI: 10.1021/jp512590z.

AUTHOR INFORMATION

Corresponding Authors
*E-mail: c.fang@uu.nl
*E-mail: m.a.vanhuis@uu.nl. Tel.: +31 30 253 2409.
Notes
The authors declare no competing financial interest.

ACKNOWLEDGMENTS

REFERENCES

(1) Huang, P. Y.; Kurasch, S.; Alden, J. S.; Shekhawart, A.; Alemi, A. A.; McEuen, P. L.; Sethna, J. P.; Kaiser, U.; Muller, D. A. Imaging Atomic Rearrangements in Two-Dimensional Silica Glass: Watching Silica's Dance. *Science* **2013**, *342*, 224–227.

(2) Aizenberg, J.; Weaver, J. C.; Thannawala, M. S.; Sundar, V. C.; Morse, D. E.; Fratzi, P. Skeleton of Euplectella sp.: Structural Hierarchy from the Nanoscale to the Macroscale. *Science* **2005**, *309*, 275–278.

(3) Grinthal, A.; Kang, S. H.; Epstein, A. K.; Aizenberg, M.; Khan, M.; Aizenberg, J. Steering Nanofibers: An Integrative Approach to Bio-Inspired Fiber Fabrication and Assembly. *Nano Today* **2011**, *7*, 35−52.

(4) Ciriminna, R.; Sciotino, M.; Alonzo, G.; de Schrijver, A.; Pagliaro, M. From Molecules to Systems: Sol-Gel Microencapsulation in Silica-Based Materials. *Chem. Rev.* **2011**, *111*, 765−789.

(5) Björkman, T.; Kurasch, S.; Lehtinen, O.; Katakaski, J.; Yzxyev, O. V.; Srivastawa, A.; Skakalova, V.; Smel, J. H.; Kaiser, U.; Krasheninnikov, A. V. Defects in Bilayer Silica and Graphene: Common Trends in Diverse Hexagonal Two-Dimensional Systems. *Sci. Rep.* **2013**, *3*, 3482.

(6) Huang, P. Y.; Kurasch, S.; Srivastava, A.; Skakalova, V.; Kotakoski, J.; Krasheninnikov, A. V.; Hovden, R.; Mao, Q. Y.; Meyer, J. C.; Smet, J.; Muller, D. A.; Kaiser, U. Direct Imaging of a Two-Dimensional Silica Glass on Graphene. *Nano Lett.* **2012**, *12*, 1081−1086.

(7) Schroeder, T.; Adelt, M.; Richter, B.; Naschitzki, M.; Bäumer, M.; Freund, H. J. Epitaxial Growth of SiO_2 on Mo(112). *Surf. Rev. Lett.* **2000**, *7*, 7−14.

(8) Weissenrieder, J.; Kaya, S.; Lu, J.-L.; Gao, H.-J.; Shaikhutdinov, S.; Freund, H.-J.; Sierka, M.; Todorova, T.; Sauer, J. Atomic Structure of a Thin Silica Film on a Mo(112) Substrate: A Two-Dimensional Network of SiO4 Tetrahedra. *Phys. Rev. Lett.* **2005**, *95*, 076103.

(9) Löffler, D.; Uhlrich, J.; Baron, M.; Yang, B.; Yu, X. Growth and Structure of Crystalline Silica Sheet on Ru(0001). *Phys. Rev. Lett.* **2010**, *105*, 146104.

(10) Lichtenstein, L.; Büchner, C.; Yang, B.; Shaikhutdinov, S.; Heyde, M.; Wlodarczyk, R.; Sauer, J.; Freund, H. The Atomic Structure of a Metal-Supported Vitreous Thin Silica Film. *Angew. Chem., Int. Ed.* **2012**, *51*, 404−407.

(11) Wulf, G. United States Patent Office 3,345,132 (Patented Cct. 3. 1967). Application Germany, June 3, 1964 W 36914, 8 Claims (Cl. 23−182).

(12) Zachariasen, W. H. The Atomic Arrangement in Glass. *J. Am. Chem. Soc.* **1932**, *54*, 3841−3851.

(13) Meyer, J. C.; Geim, A. K.; Katsnelson, M. I.; Novoselov, K. S.; Booth, T. J.; Roth, S. The Structure of Suspended Graphene Sheets. *Nature* **2006**, *446*, 60−63.

(14) van Blaaderen, A.; Ruel, R.; Wiltzius, P. Template-Directed Colloidal Crystallization. *Nature* **1997**, *385*, 321−324.

(15) Kuijk, A.; van Blaaderen, A.; Imhof, A. Synthesis of Monodisperse, Rodlike Silica Colloids with Tunable Aspect Ratio. *J. Am. Chem. Soc.* **2011**, *133*, 2346−2349.

(16) Penninkhof, J. J.; Graf, C.; Dillen, T.; van Vredenberg, A. M.; van Blaaderen, A.; Polman, A. Angle-Dependent Extinction of Anisotropic Silica/Au Core/Shell Colloids Made via Ion Irradiation. *Adv. Mater.* **2005**, *17*, 1484−1488.

(17) Mühlstein, L. A.; Sauer, J.; Bein, T. Tuning the Thermal Relaxation of a Photochromic Dye in Functionalized Mesoporous Silica. *Adv. Funct. Mater.* **2008**, *19*, 2027−2037.

(18) Fells, D. A.; Firth, J. B. The Function of Water Present in Silicic Acid Gel - The Structure of Silicic Acid Gel. *J. Phys. Chem.* **1927**, *31*, 1230−1236.

(19) Attard, G. S.; Glyde, J. C.; Göltner, C. G. Liquid-Crystalline Phases as Templates for the Synthesis of Mesoporous Silica. *Nature* **1995**, *378*, 366−368.

(20) Brinker, C. J. Hydrolysis and Condensation of Silicates: Effects on Structure. *J. Non-Cryst. Solids* **1988**, *100*, 31−50.

(21) Wang, L. S.; Nicholas, J. B.; Dupuis, M.; Wu, H.; Colson, S. D. Si_3O_y (y = 1−6) Clusters: Models for Oxidation of Silicon Surfaces and Defect Sites in Bulk Oxide Materials. *Phys. Rev. Lett.* **1997**, *78*, 4450−4453.

(22) Zhao, M. W.; Zhang, R. Q.; Xia, Y. Y.; Lee, S.-T. Structural Characterization of Fully Coordinated Ultrathin Silica Nanotubes by First-Principles Calculations. *Phys. Rev. B* **2006**, *73*, 195412.

(23) Bromley, S. T. Thermodynamic Stability of Discrete Fully Coordinated SiO_2 Spherical and Elongated Nanocages. *Nano Lett.* **2004**, *4*, 1427−1432.

(24) de Leeuw, N. H.; Du, Z. M.; Li, J.; Yip, S.; Zhu, T. Computer Modeling Study of the Effect of Hydration on the Stability of a Silica Nanotube. *Nano Lett.* **2003**, *3*, 1347−1352.

(25) Zhao, M. W.; Zhang, R. Q.; Xia, Y. Y.; Song, C.; Lee, S.-T. Faceted Silicon Nanotubes: Structure, Energetic, and Passivation Effects. *J. Phys. Chem. C* **2007**, *111*, 1234−1238.

(26) Bondi, R. J.; Lee, S. H.; Hwang, G. S. First-Principles Study of the Structural, Electronic, and Optical Properties of Oxide-Sheathed Silicon Nanowires. *ACS Nano* **2011**, *5*, 1713−1723.

(27) Stöber, W.; Fink, A.; Bohn, E. Controlled Growth of Monodisperse Silica Spheres in the Micron Size Range. *J. Colloid Interface Sci.* **1968**, *26*, 62−69.

(28) Hench, L. L.; West, J. K. The Sol-Gel Process. *Chem. Rev.* **1990**, *90*, 33−72.

(29) Dunn, B.; Zink, J. I. Probes of Pore Environment and Molecule−Matrix Interactions in Sol−Gel Materials. *Chem. Mater.* **1997**, *9*, 2280−2291.

(30) Baccile, N.; Babonneau, F.; Thomas, B.; Coradin, T. Introducing Ecodesign in Silica Sol−Gel Materials. *J. Mater. Chem.* **2009**, *45*, 8537−8559.

(31) Giraido, L. F.; Löpez, B. L.; Pérez, L.; Urrego, S.; Sierra, L.; Mssa, M. Mesoporous Silica Applications. *Macromol. Symp.* **2007**, *258*, 129−141.

(32) Buckley, A. M.; Greenblatt, M. The Sol-Gel Preparation of Silica Gels. *J. Chem. Educ.* **1994**, *71*, 599.

(33) Neugebauer, J.; Hickel, T. Density Functional Theory in Materials Science. *Wiley Interdiscip. Rev.: Comput. Mol. Sci.* **2013**, *3*, 438−448.

(34) Dion, M.; Rydberg, H.; Schröder, E.; Langreth, D. C.; Lundqvist, B. I. Van derWaals Density Functional for General Geometries. *Phys. Rev. Lett.* **2004**, *92*, 246401.

(35) Klimeš, J.; Bowler, D. R.; Michelides, A. Chemical Accuracy for the van der Waals Density Functional. *J. Phys.: Condens. Matter* **2010**, *22*, 022201.

(36) Fang, C. M.; Li, W.-F.; Koster, R. S.; Klimeš, J.; van Blaaderen, A.; van Huis, M. A. The Accurate Calculation of the Band Gap of Liquid Water by Means of GW Corrections Applied to Plane-Wave Density Functional Theory Molecular Dynamics Simulations. *Phys. Chem. Chem. Phys.* **2015**, *17*, 365−375.

(37) Tran, F.; Hutter, J. Nonlocal van der Waals Functionals: The Case of Rare-Gas Dimers and Solids. *J. Chem. Phys.* **2013**, *138*, 204103.

(38) Kresse, G.; Hafner, J. Ab Initio Molecular-Dynamics Simulation of the Liquid-Metal−Amorphous-Semiconductor Transition in Germanium. *Phys. Rev. B* **1994**, *49*, 14251−14269.

(39) Kresse, G.; Furthmller, J. Effciency of Ab-Initio Total Energy Calculations for Metals and Semiconductors Using a Plane-Wave Basis Set. *Comput. Mater. Sci.* **1996**, *6*, 15−50.

(40) Kresse, G.; Marsman, M.; Furthmüller, J. *VASP the Guide*; Universität Wien: Austria (http://cms.mpi.univie.ac.at/vasp/vasp.pdf, accessed online on April 1, 2015).

(41) Monkhorst, H. J.; Pack, J. D. Special Points for Brillouin-Zone Integrations. *Phys. Rev. B* **1976**, *13*, 5188.

(42) Painter, L. R.; Hamm, R. N.; Arakawa, E. T.; Birkhoff, R. D. Electronic Properties of Liquid Water in the Vacuum Ultraviolet. *Phys. Rev. Lett.* **1968**, *21*, 282−285.

(43) Brice, J. C. The Lattice Constants of α-Quartz. *J. Mater. Sci.* **1980**, *15*, 161−167.

(44) Becke, A. D. Density Functional Thermochemistry. III. The Role of Exact Exchange. *J. Chem. Phys.* **1993**, *98*, 5648−5652.

(45) Wigner, E. P. Uber die Erhaltungssatze in der Quanten Mechanik. *Nachr. Ges. Wiss. Goettingen, Math.-Phys.* **1927**, 375.

(46) Torun, E.; Fang, C. M.; de Wijs, G. A.; de Groot, R. A. Role of Magnetism in Catalysis: RuO_2(110) Surface. *J. Phys. Chem. C* **2013**, *117*, 6353−6357.

(47) van der Lit, J.; Boneschanscher, M. P.; Vanmaekelbergh, D.; Ijäs, M.; Uppstu, A.; Ervasti, M.; Harju, A.; Liljeroth, P.; Swart, I. Suppression of Electron−Vibron Coupling in Graphene Nanoribbons Contacted via a Single Atom. *Nat. Commun.* **2013**, *4*, 2023.